

The faithful copy neuron

Lawrence Sirovich

Received: 14 June 2011 / Revised: 19 July 2011 / Accepted: 21 July 2011
© Springer Science+Business Media, LLC 2011

Abstract Theoretical and experimental evidence is presented for the presence in nervous tissue of neurons whose firing rate faithfully follow their input stimulus. Such neurons are shown to deliver their spikes with minimum dissipation per spike. This optimal performance is likely accomplished by use of local circuitry that adjusts conductances to match input currents so that the neuron operates near the threshold for firing. This results in an unusual mechanism for neuronal firing that uses background noise to achieve the desired firing rate. This framework takes place dynamically, and the present deliberations apply under time varying conditions. It is shown that an analytically explicit probability distribution function, which depends on one dimensionless parameter, can account for the interspike interval statistics under general time varying conditions. An innovative analysis based on the unsteady firing rate fits data to the appropriate probability distribution function.

Keywords Retinal dynamics · Interspike intervals · First passage problem · Ornstein-Uhlenbeck

1 General background

In a pioneering paper Knight (1972) demonstrated conditions under which a population of noiseless encoders

can perfectly replicate an input stimulus. The present study shows that this may be a likely goal of real spiking neurons. Quantitative correspondence between theory and experiment requires a particular model, which will be taken to be the leaky-integrate-and fire neuron. Before this we make some general model-free observations.

A spiking neuron is characterized by its neuronal membrane potential V which varies between the resting state V_r and the threshold for firing a spike V_t and conveniently parameterized by

$$x = \frac{V - V_r}{V_t - V_r} \quad (1)$$

with

$$-\infty \leq x \leq 1. \quad (2)$$

Within this framework a neuron fires a spike when x reaches unity after which the neuron returns to the resting state, $x = 0$. The interval has been extended to $-\infty$ to account for inhibition and noise.

In a typical laboratory experiment successive spike times $\{t_j\}$ are collected. Troy and Robson (1992) have demonstrated that to good approximation this represents a renewal process, i.e., memory plays no role. With the exception of noise the next spike time t_j only depends on conditions at t_{j-1} and the intervening current; the interspike interval (t_j, t_{j-1}) will be denoted by

$$t_j^I = t_j - t_{j-1}. \quad (3)$$

The superscript I will be used to distinguish interspike time from elapsed time.

Microelectrode recordings of neuronal activity lead to the determination of three macroscopic parameters:

Action Editor: Jonathan David Victor

L. Sirovich (✉)
Laboratory of Applied Mathematics, Mount Sinai
School of Medicine, One Gustave L. Levy Place,
New York, 10029 NY, USA
e-mail: lsirovich@rockefeller.edu

current input from local circuitry to the neuron, s ; a coefficient of current leakage (conductance), γ ; and the internal noise level measured by a diffusion coefficient, D . Under the parameterization Eq. (1) each of these three quantities has the physical units of inverse time, i.e., each is a frequency.

A spiking neuron responds to stimulation by firing a train of spikes, characterized by a time dependent firing rate $J(t)$, also of frequency units. Within the present framework J is a function of s , γ and D and elementary dimensional analysis dictates that there exists a function κ such that

$$J/s = \kappa(\epsilon, \hat{s}) \quad (4)$$

where

$$\epsilon = D/s \quad (5)$$

and

$$\hat{s} = s/\gamma, \quad (6)$$

are dimensionless quantities. The experimentally determined peri stimulus time histogram PSTH produces a firing rate that we will use for data analysis. This is non-differentiable and smoother versions have been proposed (Knight 2008; Behseta et al. 2003).

A PSTH is derived by binning the interspike intervals, t^I and is thus related to the instantaneous firing rate $1/t^I$. In such terms dimensional reasoning implies

$$t^I = \frac{1}{s\kappa(\epsilon, s/\gamma)}, \quad (7)$$

where this might be a different κ . On the basis of the renewal property of spike arrival times t^I depends on the values of (s, γ, D) after the previous spike. If these parameters do not vary drastically during the interspike interval then Eq. (7), and hence Eq. (4), can be regarded as reasonably describing the time varying case. A recent analysis of laboratory data (see Casti et al. 2008; Knight 2008) provides evidence that Eq. (4) holds for robust variation, and that \hat{s} and ϵ remain constant (Sirovich and Knight 2011). Since $\gamma \neq 0$ for $s \rightarrow 0$, our discussion will only apply suitably above the noise floor, $s > 0$.

In what follows evidence in support of this framework will be marshalled, and consequences of the assertion developed.

1.1 Time dependent case

To treat the general time dependent case it proves convenient to consider a *modified clock*. The natural clock suggested by data differs from a theoretically

more convenient clock, and the reader is alerted to this distinction. As will be seen the transformation

$$\tilde{\tau}(t) = \int_0^t J(t')dt', \quad (8)$$

where $t = 0$ is a convenient origin, is natural for data analysis. For example if T is the duration of the experiment then

$$\tilde{\tau}(T) = \int_0^T J(t')dt' = \tilde{N} \quad (9)$$

is the probable number of spikes in the interval $(0, T)$, and the integral of $J(t)$ over any time interval yields the probable number of spikes occurring in that interval. Hence the probable interspike interval in $\tilde{\tau}$ -space is

$$\tilde{\tau}_j^I = \int_{t_{j-1}}^{t_j} J(t')dt', \quad (10)$$

which for a large enough ensemble $\{t_j\}$ has unit mean.

The Meyer-Papangelou time-rescaling theorem is based on a similar clock transformation. As demonstrated in Brown et al. (2001) this transforms a wide variety of inhomogeneous data types that involve counting events into a standard Poisson process of unit mean; however this is not the present perspective. As will be seen the collection

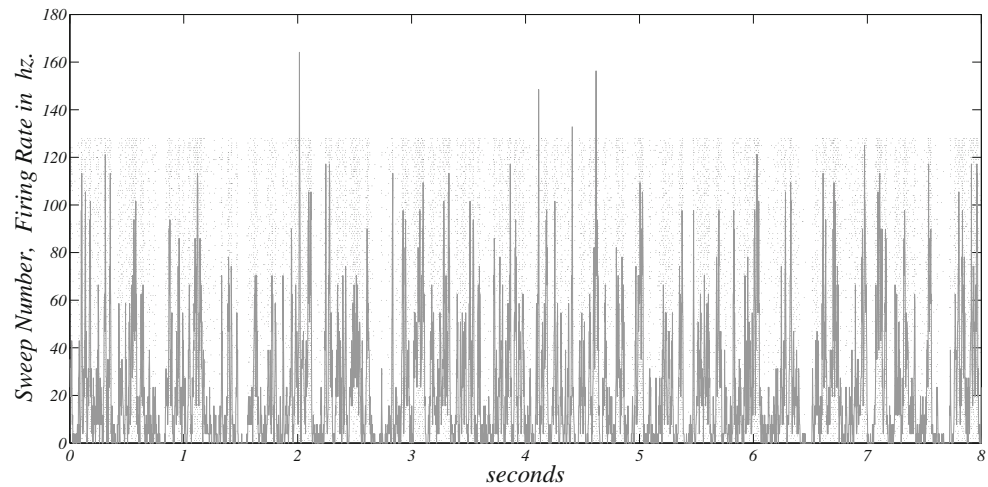
$$\{\tilde{\tau}_j^I\} \quad (11)$$

generated by Eq. (10) will identify the appropriate pdf by which to describe the data.

Comparison with experiment will be based on an extensive collection of physiological data (Casti et al. 2008; Knight 2008; Casti et al. 2011). In the experiments the retinal ganglion cell (RGC) firings are recorded at the lateral geniculate nucleus (LGN) (Bishop 1953; Kaplan and Shapley 1984; Ozaki and Kaplan 2006) of cat in response to uniform spots of illumination that rapidly vary in luminance in a way that is related to naturalistic light changes (van Hateren 1997). In a typical experiment roughly 23,000 spikes are recorded during 128 repeats of 8 s of one temporal series of illuminations. (In the experiments these presentations were interleaved with randomly chosen 8 s unique segments, not discussed here). In Fig. 1 the raster plot of one such case of spike times appears as a gray dust. In addition we show the firing rate calculated from the PSTH which sampled the 8 s record with 8,000 bins and hence with a resolution of 1 ms.

In Fig. 2 we show the PSTH of Fig. 1 displayed as a probability. Bin width was chosen according to the Freedman-Diaconis rule (Freedman and Diaconis 1981). The theoretical curve that is shown will be discussed later corresponds to $s/\gamma = 1$ and $\epsilon = 0.2$.

Fig. 1 The collection of spike times for the 128 repeats of a 4.25° spot size is shown as a raster plot with sweeps 1,2,...128. The continuous curve represents the PSTH experimental firing rate $J(t)$ calculated by using 1 ms bins. Note that the ordinate accounts for both firing rate in hz and sweep number, which for this data set have comparable range



A high resolution collection of analytically derived interspike interval (ISI) pdfs

$$\{\mathcal{P}(\tilde{\tau}^I; \epsilon, \hat{s})\}, \quad (12)$$

were generated by methods described in the Appendix. Data analysis is based on best fit, in the least squares sense, of the data-generated pdf, Eq. (11), to the collection Eq. (12). This fit determines ϵ and \hat{s} , and from this $s(t)$, $\gamma(t)$ and $D(t)$.

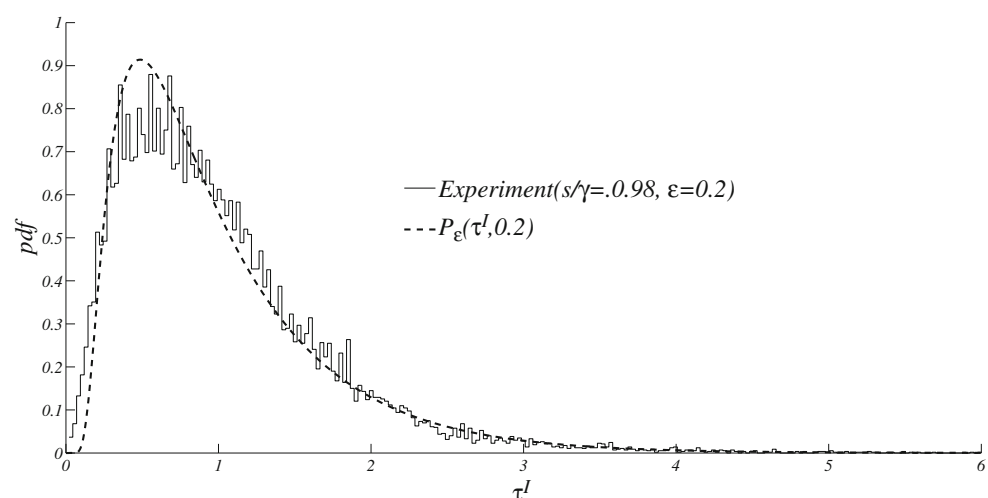
As is clear from Fig. 2, even with the ideal bin width of the Freedman & Diaconis-rule (Freedman and Diaconis 1981), for the over 23,000 spikes of the ensemble, the pdf is somewhat ragged, and outliers appear at both ends of the intervals. To overcome the raggedness we adopt a fitting procedure based on matching the cumulative distribution function (cdf) of data to a theoretical cdf which is related to the Kolmogorov-Smirnov fit (Lupton 1993). In brief for interspike

intervals $\{\tilde{\tau}_j^I\}$, $j = 1, \dots, N$ is normalized such that the average $\langle \tilde{\tau}_j^I \rangle_j = 1$ and the experimental cdf,

$$C_E = \frac{1}{N} \sum_{j=1}^N \delta(\tau - \tilde{\tau}_j^I) \quad (13)$$

is formed. This is then fit to the best theoretical counterpart on the basis of the distance to the theoretical cdfs at 511 equal locations on the C -axis, $0 < C < 1$ using a least square fit. In prior analyses (Casti et al. 2008; Knight 2008; Sirovich and Knight 2011) a phase plane ($J(t), \dot{J}(t)$) of experimental data was constructed, and divided into 21 coarse grained compartments, based on seven levels of J and $\dot{J} < 0, \dot{J} \approx 0, \dot{J} > 0$. Since each compartment contained roughly 1100 spike intervals the counterpart of Fig. 2 becomes rougher and an intrinsically defined filter was additionally introduced to minimize the contribution of outliers (Sirovich and Knight 2011).

Fig. 2 The stairs plot the experimental histogram; the dotted curve is the theoretical pdf for $s/\gamma = 1$ and $\epsilon = 0.2$, which differs slightly from the theoretical pdf for the experimental parameters



1.2 Faithful copy neuron

A central result of the prior work was that both ϵ and \hat{s} appear to be constant for a substantial portions of the data and moreover that

$$\hat{s} \approx 1. \quad (14)$$

A theoretical demonstration of the constancy of ϵ based on Campbell's theorem (Rice 1944), is shown in (Knight et al. 1996). The constancy of \hat{s} suggests that γ the membrane conductivity also varies with time, as suggested by Koch et al. (1996). Amongst other possibilities this would be consistent with the notion that synaptic arrivals open channels that are also sources of leakage. The constancy of \hat{s} has been shown to follow from an analytical model (Nykamp and Tranchina 2000) under the limit of fast synaptic dynamics (Dan Tranchina, private communication). The Discussion section presents a demonstration that Eq. (14) produces minimum dissipation per spike delivered.

For constant ϵ and \hat{s} given by Eq. (14) it follows that the firing rate J is proportional to the stimulus which from Eq. (4) is

$$J(t) = \kappa(\epsilon, 1)s(t). \quad (15)$$

with the coefficient κ a constant. Clearly this is an instance of the firing rate following the stimulus, and so produces a faithful copy of s .

1.3 Leaky-integrate-and-fire model

The above considerations have been developed under general conditions; to proceed quantitatively the leaky integrate-and-fire neuron model

$$\frac{dx}{dt} = -\gamma x + s \quad (16)$$

Fig. 3 The heavy continuous curve, $\epsilon = 0$, represents the deterministic firing rate of Eq. (16), while the dashed line indicates that the solution $x = s/\gamma > 1$ is unstable. Other curves show firing rates for $\epsilon > 0$

is adopted. This has proven to be a remarkably good approximation to the Hodgkin-Huxley model if spike duration times are short compared to interspike times (Knight 1972; Dayan and Abbott 2001; Carrillo and Hoppensteadt 2010).

Equation (16) is to be solved under the condition that x is reset to rest, $x = 0$, on firing a spike, $x = 1$, a non-linear framework. For Eq. (16) considered as a dynamical system, \hat{s} is the equilibrium and also the bifurcation parameter. The system undergoes bifurcation at the critical point

$$\hat{s} = 1, \quad (17)$$

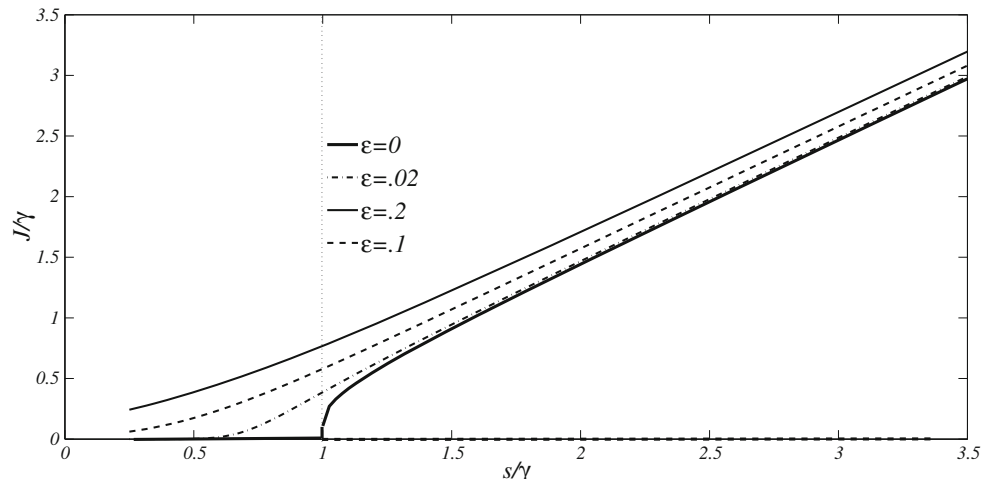
from a stable equilibrium for $\hat{s} < 1$ and to unstable equilibrium for $\hat{s} > 1$, leading to limit cycle periodic firing.

The normalized firing rate, J/γ , the heavily drawn curve in Fig. 3 thus provides a suitable bifurcation diagram.

The deterministic view for this system substantially changes with the addition of noise. An appropriate stochastic extension of Eq. (16) is furnished by the Ornstein-Uhlenbeck equation (Smoluchowski 1915; Schrödinger 1915; Uhlenbeck and Ornstein 1930; Gardiner 2009).

$$\frac{\partial \rho(x, t)}{\partial t} = \frac{\partial}{\partial x} \left\{ (\gamma x - s)\rho(x, t) + D \frac{\partial}{\partial x} \rho(x, t) \right\} \quad (18)$$

for the probability density function $\rho(x, t)$ that the membrane potential is x at time t (Knight et al. 1996). The steady state of Eq. (18) can be formulated and easily solved (Sirovich et al. 2000) to give firing rates; examples are shown in Fig. 3. As seen there stochasticity overcomes the deterministic threshold barrier at $s/\gamma = 1$. Thus the addition of noise is a facilitator that



allows the neuron to jump the threshold and fire an impulse.

The interspike interval pdf, through standard arguments, can be reduced to the first passage problem of Eq. (18) that places an initial delta function at $x = 0$, and places an absorbing boundary condition at $x = 1$.

As shown in the Appendix the solution of the first passage can be reduced to an integral equation that can be easily solved numerically. In one, very important instance, there exists an exact solution (Ricciardi 1977; Sampath and Srinivasan 1977). If $s/\gamma = 1$ (whence $\beta = 0$) the interspike pdf is

$$\mathcal{P}_\epsilon(\tau^I; \epsilon) = \sqrt{\frac{2}{\pi\epsilon}} \frac{e^{-\tau^I}}{(1 - e^{-2\tau^I})^{3/2}} \exp\left(-\frac{e^{-2\tau^I}}{2\epsilon(1 - e^{-2\tau^I})}\right). \quad (19)$$

This depends on the single dimensionless parameter ϵ , and in the following will be referred to as the ϵ -distribution or ϵ -pdf.

1.4 Synthetic data

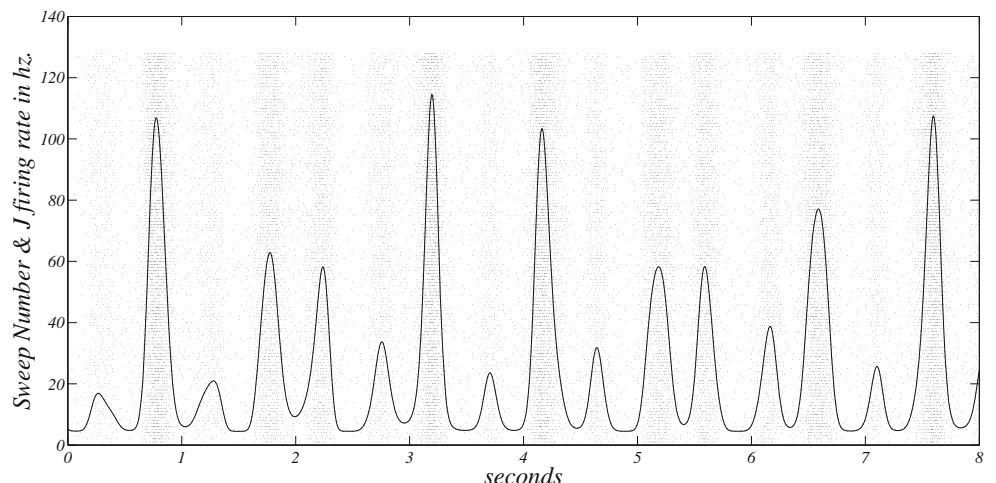
To mimic physiological experiments we chose the stimulus $s^o(t)$ indicated by the curve in Fig. 4, with a duration of 8 s.

$\epsilon = .19$ and $\hat{s} = 1$ ($\beta = 0$) were chosen to be in approximate agreement with experiments that will be considered. The firing rate shown in Fig. 4 is

$$J = \kappa(.19, 1)s^o(t) \quad (20)$$

with $s^o(t)$ chosen to be a pseudo-random admixture of 4 incommensurate frequencies so that J ranged roughly between 5 and 115 hz.

Fig. 4 Synthetic data, see figure legend of Fig. 1



A pseudo experiment is then generated by randomly choosing an appropriate collection of interspike intervals

$$\{\tau_j^I\}, j = 1, \dots, N \quad (21)$$

from the ϵ -distribution

$$\mathcal{P}_\epsilon(\tau; .19). \quad (22)$$

Successive firing times t_j are then generated by solving

$$\tau_j^I = \int_{t_{j-1}}^{t_j} s^o(t') dt' = \frac{1}{\kappa} \int_{t_{j-1}}^{t_j} J(t') dt' \quad (23)$$

for t_j . In practice N in Eq. (21) is chosen larger than needed and the actual number of spikes is then determined by trimming the number of spikes from Eq. (23) so that $t = 8$ s is not exceeded.

Following laboratory protocol this procedure was performed 128 times using the same stimulus; altogether about 23,000 spikes were collected. The background gray dust in Fig. 4 is the raster plot of all the generated spikes. The approximate firing rate was created by forming a histogram of 1,600 bins for the 8 s and which leads to an excellent fit to $s^o(t)$.

As a test of the procedure and the algorithm to be applied to experimental data we regard the data just generated as a data set of spike times $\{t_i\}$. The corresponding interspike intervals $\{\tau_j^I\}$ follows from Eq. (3). We then attempt to recover the parameters and time histories from these roughly 23,000 data points.

As a first step we repeat the construction of the approximate $J_\epsilon(t')$, since this only depends on the spike times $\{t_i\}$. Next we return to Eq. (10) from which we construct the ensemble of interspike interval times

$$\{\tilde{\tau}_j^I\}. \quad (24)$$

Table 1 As indicated the second of each pair of results indicates the fit to the ϵ -pdf

Spot size/deg.	ϵ	s/γ	β	Error	J, hz.
4.25°	0.21	1.03	0.08	0.028	22.59
4.25°	0.20	1	0	0.028	22.59
2.65°	0.24	1.29	0.59	0.032	21.81
2.65°	0.16	1	0	0.032	21.81
2.12°	0.24	1.39	0.79	0.035	22.97
2.12°	0.14	1	0	0.035	22.97
1.60°	0.24	1.42	0.87	0.033	23.32
1.60°	0.13	1	0	0.038	23.32
1.06°	0.27	2.04	2.01	0.032	27.82
1.06°	0.08	1	0	0.04	27.82
0.53°	0.20	0.87	-0.28	0.024	17.85
0.53°	0.25	1	0	0.024	17.85

The error column is based on the fractional rms departure

We then interrogate the full collection of ISI pdfs discussed above to obtain the best mean square fit of these data to the theoretical pdfs. The result of this is determinations

$$\epsilon = .19 \text{ and } \hat{s} = .9956, \quad (25)$$

in excellent agreement with the exact result of $\epsilon = .19$ & $\hat{s} = 1$.

Finally from Eq. (39) we determine

$$\kappa = 1/(\hat{s}\langle\tau^I\rangle); \quad (26)$$

which gives

$$\hat{s} = J(t)/\kappa. \quad (27)$$

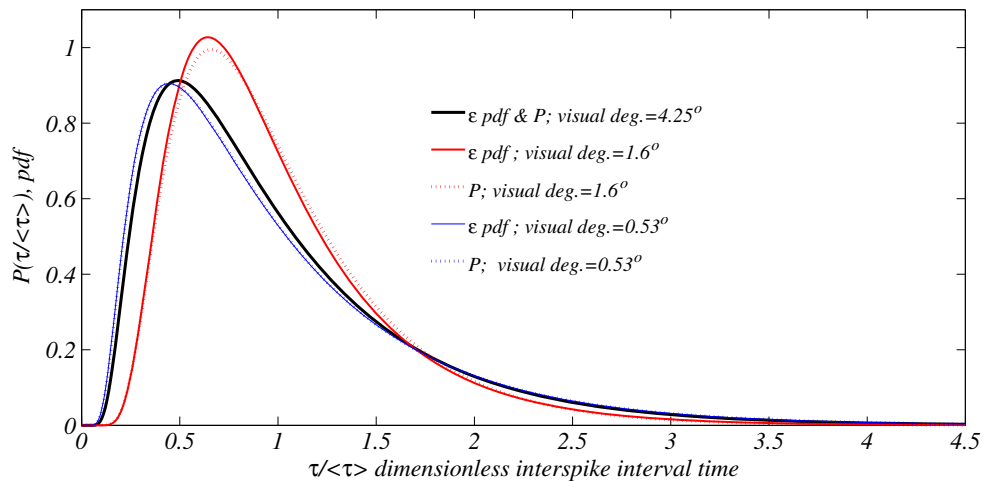
the driving current.

2 Application to experiment

Figure 1 depicts responses of an off-center X retinal ganglion cell (RGC). These cells have circular center surround organization with excitatory centers and inhibitory concentric surrounds. In particular Fig. 1 is the record from a circular spot of illumination of 4.25° (visual degrees), which encompasses more than the full center-surround organization. Five additional cases ranging from 4.25° to .53° visual degrees were considered during this experiment (Casti et al. 2008; Knight 2008; Casti et al. 2011). The results of applying the above analysis for all cases is summarized in Table 1.

In each instance the data were analyzed by applying the full collection of pdfs Eq. (12) and the ϵ -pdfs Eq. (19). Pdfs of Eq. (12) show ribbons of near pdfs in the ϵ - β plane (Sirovich and Knight 2011), and evidence of such aliases can be seen in the Table. For 4.25° the two fits are in agreement, a slight difference in error is

Fig. 5 Comparison of \mathcal{P} , Eq. (12), and ϵ -pdfs, Eq. (19). For $SS = 4.25^\circ$, black line, the two are indistinguishable; this is also virtually true for $SS = .53^\circ$; the exception is $SS = 1.6^\circ$ discussed in the text



not shown. With the exception of 1.06° all cases appear to be well described by the ϵ -distribution.

In Fig. 5 we show the comparison of pdfs for 4.25° , 1.06° , $.53^\circ$, and as anticipated by the errors shown in the Table 1.06° is the only case that shows a significant deviation.

1.06° coincides with the center region (Alex Casti, private communication), a fact that is supported by the observation that this case has the highest firing rate. Although an effort is made in experiments to immobilize the eye this is only partially successful. Some saccadic movement is still present and this may account for the error that occurs for 1.06° (Ehud Kaplan, private communication).

Since the analysis procedure is based on the assumption of constancy of ϵ and \hat{s} , Eqs. (5) and (6), one may question whether the faithful copy property is really present or being forced by the data analysis. This issue was addressed in the coarse grained analysis discussed above Sirovich and Knight (2011) which showed that most ranges produced $s/\gamma \approx 1$ and $\epsilon \approx .19$.

Another perspective is that $\mathcal{P}_\epsilon(\tau; 0.2)$ used with the current as shown in Fig. 1, produces *synthetic data* that agrees with physiological experiment, suggests a lack of uniqueness. As shown in the Discussion the faithful copy produces the least energy dissipation for spikes delivered. It is a speculation that this implies that the faithful copy neuron (FCN) is unique in producing the best least squares fit.

3 Discussion

Over the hundreds of millions of years of visual evolution optimization can be assumed to have played a role. To pursue this within the present framework consider the stochastic leaky-integrate-and fire model

$$\frac{dx}{dt} = -\gamma x + h \sum_j \delta(t - t_j^a) \quad (28)$$

with synaptic arrival times $\{t_j^a\}$ over some period $0 \leq t_j \leq T$ and so that arrivals produce small membrane potential jumps h . The current $s(t)$ that appears in Eq. (16) is defined by

$$s(t) = \left\langle h \sum_{j=1} \delta(t - t_j^a) \right\rangle \quad (29)$$

for a suitably defined ensemble average. In Omurtag et al. (2000) it is shown that Eqs. (28) and (29) produce Eq. (18), in the limit of small jump size h . Synaptic arrival times (to the retinal ganglion cell) should not be confused with the firing times and the superscript un-

derlines this distinction. While $s(t)$ defined by Eq. (29) is the current, the synaptic arrival rate is $s(t)/h$. An estimate in retina of this rate is furnished by the value $h = 1/10$ (Freed 2005).

In the spirit of Langevin's analysis of Brownian motion (Gardiner 2009), Eq. (28) is multiplied by x and the result is then averaged over a suitable ensemble to obtain

$$\frac{1}{2} \frac{d}{dt} \langle x^2 \rangle = \langle (s - \gamma x) x \rangle + \langle x \mu(t) \rangle, \quad (30)$$

where

$$\mu(t) = h \sum_j \delta(t - t_j^a) - s(t) \quad (31)$$

is the residual noise. Following Langevin the last term Eq. (30) may be reasonably regarded as negligible since $\mu(t)$ is rapidly varying and of zero mean and thus

$$\frac{1}{2} \frac{d}{dt} \langle x^2 \rangle \approx \langle (s - \gamma x) x \rangle. \quad (32)$$

For $s > \gamma$, Eq. (32) implies that dissipation grows with time, since the righthand side is positive. If s is well below γ the neuron is unlikely to fire and will not accomplish its signaling role. This suggests that evolution might choose $\gamma \lesssim s$ which since $\langle x^2 \rangle$ is proportional to (ohmic) dissipation yields the least energy dissipation for spikes delivered. In this case the leaking current matches the input stimulus and the neuron spends most of its time lingering near threshold

$$\langle x^2 \rangle \approx 1, \quad (33)$$

a result which might lend itself to experimental verification; and consistent with the assertion that the last term of Eq. (30) is negligible.

In this case the dissipation is constant, Eq. (33), and the neuron signals its output $J(t)$ by using the available intrinsic noise to reach threshold. Thus the flux of noise which is also carried by s is responsible for threshold crossing and yields Eq. (15) as exemplified by Eq. (20).

In somewhat more detail fluctuations in a neural micro-circuit are described by Johnson/Nyquist noise (Johnson 1928; Nyquist 1928), a temperature dependent effect. Voltage fluctuations result from Brownian behavior in the ionic current source. The present analysis suggests that the FCN evolved by exploiting the available noise as a means of overcoming the firing threshold. Being within 1% of threshold, as suggested by the data, translates into roughly .5 mV, which is also a nominal estimate of Johnson/Nyquist voltage fluctuations. Evolution might choose this over driving a neuron by current increase which is metabolically costly and heat producing. This unusual mechanism might

also be regarded as a variation on stochastic resonance (Bulsara and Gammaitonni 1996). Since a spike is a source of information there is room for speculation on whether the FCN might also extremize information per spike.

As observed $s/\gamma = 1$ is a critical point of the dynamical system, Eq. (14), becomes an attractor of the system. In the literature such phenomena have been referred to as self-organized criticality (Kadanoff et al. 1989; Bak and Paczuski 1995).

Biological systems have many instances of thresholds in the presence of noise, and since biology is known to repeat its *tricks* in different guises the present formalism may have wider significance.

Only several cases of one set of many experiments of Casti et al. (2008, 2011) and Knight (2008) has been analyzed in depth here, however preliminary analysis of a significant fraction of these data sets shows consistency with the faithful copy neuron. Should this pattern of agreement hold it lends importance to the one parameter ϵ -distribution (Eq. (19)) presented here.

Acknowledgements It is a pleasure to acknowledge my interactions with my longtime collaborator Bruce Knight. Thanks are also in order for the helpful comments of Udi Kaplan, Alex Casti, Charlie Peskin, Dan Tranchina, and Jonathan Victor. Thanks also to Alex Casti for allowing use of his hard gained data. I also thank Ellen Paley for her careful help in the preparation of this paper and for her great patience with the many drafts that preceded this one. Support for this work came from NIH/NEI EY16224 and NIH/NIGMS P50 GM071558.

Appendix: General case

Instead of the spike counting clock (Eq. (8)), Eq. (18) is more suitably transformed by

$$\tau(t) = \frac{1}{\bar{s}} \int_0^t s(t') dt'. \quad (34)$$

In addition we write

$$x = 1 - \sqrt{\epsilon} z \quad (35)$$

and

$$\beta = (\bar{s} - 1)/\sqrt{\epsilon} \quad (36)$$

so that Eq. (18) becomes

$$\frac{\partial \rho}{\partial \tau} = \frac{\partial}{\partial z} \left[(z + \beta) \rho + \frac{\partial \rho}{\partial z} \right]; 0 \leq z \leq \infty, \quad (37)$$

Sirovich and Knight (2011). The time transformation (Eq. (34)) uses $\gamma(t)$ as a temporal density in order to

achieve the form of Eq. (37). Observe that the interspike interval based on Eq. (34), τ^I satisfies

$$\kappa \hat{s} \tau^I = \tilde{\tau}^I, \quad (38)$$

and an immediate consequence is

$$\langle \tau^I \rangle = 1 / (\hat{s} \kappa(\epsilon, \hat{s})). \quad (39)$$

In terms of Eq. (37) the initial condition becomes

$$\rho(z, \tau = 0) = \delta(z - 1/\sqrt{\epsilon}) \quad (40)$$

and the absorbing boundary condition is now at the origin

$$\rho(0, \tau) = 0. \quad (41)$$

Using standard arguments the interspike interval pdf is given by

$$\mathcal{P}(\tau^I; \beta, \epsilon) = \frac{\partial}{\partial z} \rho(z, \tau^I; \beta, \epsilon) \Big|_{z=0} \quad (42)$$

where ρ is the solution to the above stated problem. It can be shown (Sirovich and Knight 2011) that $\mathcal{P}(\tau)$ (Eq. (42)) satisfies

$$\frac{e^{(e^{-\tau^I}/\sqrt{\epsilon} - a(\tau^I))^2/2v(\tau^I)}}{\sqrt{2\pi v(\tau^I)}} = \int_0^{\tau^I} d\sigma \frac{e^{-a(\sigma)^2/2v(\sigma)}}{\sqrt{2\pi v(\sigma)}} P(\tau - \sigma) \quad (43)$$

where

$$a(\tau) = \beta(1 - e^{-\tau}) \quad (44)$$

and

$$v(\tau) = 1 - e^{-2\tau} \quad (45)$$

Equation (43), a convolution Volterra equation, can be solved numerically with ease, and one can easily build up an extensive class of interspike interval pdfs. For data analysis roughly 142,000 pdfs covering $-3 \leq \beta < 3$, $.01 < \epsilon < .6$ in increments of 0.005 were constructed. This construction, based on an enhanced trapezoidal rule, led to the high resolution collection Eq. (12) mentioned earlier. The algorithm when tested against the exact result, Eq. (19), showed a fractional error of $0(10^{-5})$.

References

- Bak, P., & Paczuski, M. (1995). Complexity, contingency, and criticality. *Proceedings of the National Academy of Sciences of the United States of America*, 92, 6689–6696.

- Behseta, S., Kass, R., & Wallstrom, G. (2003). Mapping multiple features in the population response of visual cortex. *Nature*, 423, 986–990.
- Bishop, P. (1953). Synaptic transmission; an analysis of the electrical activity of the lateral geniculate nucleus in the cat after optic nerve stimulation. *Proceedings of the Royal Society of London. Series B, Biological Sciences*, 141, 362–392.
- Brown, E., Barbieri, R., Ventura, V., Kass, R., & Frank, L. (2001). The time-rescaling theorem and its application to neural spike train data analysis. *Neural Computation*, 14, 325–346.
- Bulsara, A., & Gammaitoni, L. (1996). Tuning into noise. *Physics Today*, 49, 39–45.
- Carrillo, H., & Hoppensteadt, F. (2010). Unfolding an electronic integrate-and-fire circuit. *Biological Cybernetics*, 102, 1–8.
- Casti, A., Crumiller, M., Shirvarkar, P., Kaplan, E., & Knight, B. (2008). *The perfect copy neuron* (p. 568.3). Society for Neuroscience Abstracts.
- Casti, A., Crumiller, M., Kaplan, E., Knight, B., Shirvarkar, P., & Sirovich, L. (2011). Quantitative physiology hidden in spiking responses to ‘naturalistic’ stimuli (in preparation).
- Dayan, P., & Abbott, L. (2001). *Theoretical neuroscience: Computational and mathematical modeling of neural systems*. MIT Press.
- Freed, M. (2005). Quantal encoding of information in a retinal ganglion cell. *Journal of Neurophysiology*, 94, 1048–1056.
- Freedman, D., & Diaconis, P. (1981). On the histogram as a density estimator: L2 theory. *Probability Theory and Related Fields*, 57, 453–476.
- Gardiner, C. (2009). *Handbook of stochastic methods*. Berlin: Springer.
- Johnson, J. (1928). Thermal agitation of electricity in conductors. *Physical Review*, 32, 97–109.
- Kadanoff, L., Nagel, S., Wu, L., & Zhou, S.-M. (1989). Scaling and universality in avalanches. *Physical Review. A*, 39, 6524–6537.
- Kaplan, E., & Shapley, R. (1984). The origin of the S (slow) potential in the mammalian lateral geniculate nucleus. *Experimental Brain Research*, 55, 111–116.
- Knight, B. (1972). Dynamics of encoding in a population of neurons. *Journal of General Physiology*, 59, 734–766.
- Knight, B. (2008). Some hidden physiology in naturalistic spike rasters. The faithful copy neuron. In *Brain connectivity workshop*. Australia: University of New South Wales.
- Knight, B., Manin, D., & Sirovich, L. (1996). Dynamical models of interacting neuron populations. In E. C. Gerf (Ed.), *Symposium on robotics and cybernetics: Computational engineering in systems applications*. Lille, France: Cite scientifique.
- Koch, C., Rapp, M., & Segev, I. (1996). A brief history of time (constants). *Cerebral Cortex*, 6, 93–101.
- Lupton, R. (1993). *Statistics in theory and practice*. Princeton, New Jersey: Princeton University Press.
- Nykamp, D., & Tranchina, D. (2000). A population density approach that facilitates large-scale modeling of neural networks: Analysis and an application to orientation tuning. *Journal of Computational Neuroscience*, 8, 19–50.
- Nyquist, H. (1928). Thermal agitation of electric charge in conductors. *Physical Review*, 32, 110–113.
- Omurtag, A., Knight, B., & Sirovich, L. (2000). On the simulation of large populations of neurons. *Journal of Computational Neuroscience*, 8, 51–63.
- Ozaki, T., & Kaplan, E. (2006). Brainstem input modulates globally the transmission through the lateral geniculate nucleus. *International Journal of Neuroscience*, 116, 247–264.
- Ricciardi, L. (1977). *Lecture notes in biomathematics: Diffusion processes and related topics in biology*. Springer.
- Rice, S. (1944). Mathematical analysis of random noise. *Bell System Technical Journal*, 23, 282.
- Sampath, G., & Srinivasan, S. (1977). *Lecture notes in biomathematics: Stochastic models for spike trains of single neurons*. Springer.
- Schrödinger, E. (1915). Zur theorie der fall- und steigversuche an teilchen mit brownscher bewegung. *Physikalische Zeitschrift*, 16, 289–295.
- Sirovich, L., & Knight, B. (2011). Spiking neurons and the first passage problem. *Neural Computation*, 23, 1675–1703.
- Sirovich, L., Knight, B., & Omurtag, A. (2000). Dynamics of neuronal populations: The equilibrium solution. *SIAM Journal on Applied Mathematics*, 60, 2009–2028.
- Smoluchowski, M. (1915). Notizuber die berechnung der brown-schen molkularbewegung bei des ehrenhaft-millikanen versuchsanordnung. *Physikalische Zeitschrift*, 16, 318–321.
- Troy, J., & Robson, J. (1992). Steady discharges of X and Y retinal ganglion cells of cat under photopic illuminance. *Visual Neuroscience*, 9, 535–553.
- Uhlenbeck, G., & Ornstein, L. (1930). On the theory of Brownian motion. *Physical Review*, 36, 823–841.
- van Hateren, J. (1997). Processing of natural time series of intensities by the visual system of the blowfly. *Vision Research*, 37, 3407–3416.